

Radiation of a Charge in Dielectric Concentrator for Cherenkov Radiation: Off-Axis Charge Motion

Sergey N. Galyamin,^{*} Viktor V. Vorobev, and Andrey V. Tyukhtin

Saint Petersburg State University, 7/9 Universitetskaya nab., St. Petersburg, 199034 Russia

(Dated: December 3, 2023)

A theoretical investigation of radiation field produced by a charge moving through the dielectric concentrator for Cherenkov radiation is performed for the general case where a charge trajectory is shifted with respect to the target axis. The idea of dielectric target with specific profile of the outer surface was presented and investigated in our previous papers for the symmetric case. Here we show how non-symmetric field components generated in the bulk of target affect field distribution near the focus where strong concentration of the energy occurs. Possible applications of this target are discussed.

I. INTRODUCTION

Uniform passage of a charged particle in dielectric medium with velocity exceeding that of light in this medium is accompanied by Cherenkov radiation discovered in 1937 [1] and theoretically interpreted at the same year [2]. Since that time this effect is widely used in various areas of physics [3, 4] including relatively novel medical applications based on Cherenkov radiation in biological tissues [5, 6].

Today several modern trends based on beam-dielectric interaction exist in accelerator physics. First, one should mention dielectric wakefield acceleration technique which is now operating with Terahertz (THz) wakefields [7–9] and has demonstrated Gigavolt per meter fields [10]. With this scheme, dielectric-lined waveguides (or metalized capillaries) of various transverse cross-section are utilized, i.e. closed structures with dielectric. Second, similar waveguide structures loaded with dielectric are considered nowadays as prospective candidates for contemporary beam-driven sources of THz radiation [11–15]. As was shown, with proper electron beam and dielectric structure an extraordinary THz radiation peak power can be potentially obtained [10].

On the other hand, various opened dielectric structures (without metallization at the outer surface) are extensively studied nowadays in view of development of both beam-driven radiation sources (mainly in THz range) and non-invasive systems for bunch diagnostics (including large-scale facilities such as LHC). Diagnostics systems based on Cherenkov radiation from prolonged dielectric targets possess several advantages compared to traditional schemes based on transition or diffraction radiation. For example, a prismatic dielectric target was used in a series of experiments [16–19] where prominent possibilities to use this scheme for beam position monitoring for high-energy electron and hadron beams were demonstrated. Moreover, as was shown, both mentioned prismatic target and hollow conical target can be a pow-

erful source of radiation (including THz range) [17, 20–22].

Though theory of Cherenkov radiation in infinite (semi-infinite) dielectric media and dielectric-lined waveguide structures is well developed [23–25], rigorous theoretical explanation of the radiation processes emerging during the interaction of charged particle with dielectric object of finite size (such as prismatic or hollow conical targets mentioned above) is extremely complicated. Therefore various approximate methods for calculation of radiation field are developed [16, 26–31]. One of them is our original combined approach based on exact solution of certain “etalon” problem and consequent taking into account the outer boundary using ray-optics laws and Stratton-Chu formulas [32–37]. It is worth noting that recent papers [36, 37] dealt with conical and prismatic objects which are of essential interest today due to the aforementioned applications.

The main advantage of this combined approach is its asymptotic accuracy with respect to ratio between the wavelength and the size of the target. Equally important is the fact that this method has been recently approved by numerical simulations in COMSOL Multiphysics [38]. Concerning the topic of the present paper, the discussed approach was utilized to find the outer profile of the axisymmetric dielectric target concentrating the majority of generated Cherenkov radiation (CR) in a small vicinity of a predetermined focus point without any additional lenses or mirrors [33]. This target was called “dielectric concentrator for CR” and was investigated in details for symmetric case (a charge flights along the target symmetry axis), including the study of sensitivity with respect to the charge velocity [38–40]. However, for practical realization it also important to analyze the influence of trajectory offset from the symmetry axis to the radiation characteristics, which is the main goal of the paper.

The paper is organized as follows. In Sec. II, we formulate the problem for the EM radiation from a shifted moving charge in a concentrator for CR. Application of Stratton-Chu formulas is presented in Sec. III while rigorous solution of “etalon” problem has moved to Appendix A. Section IV contains numerical results and discussion. Section V finishes the paper.

^{*} s.galyamin@spbu.ru

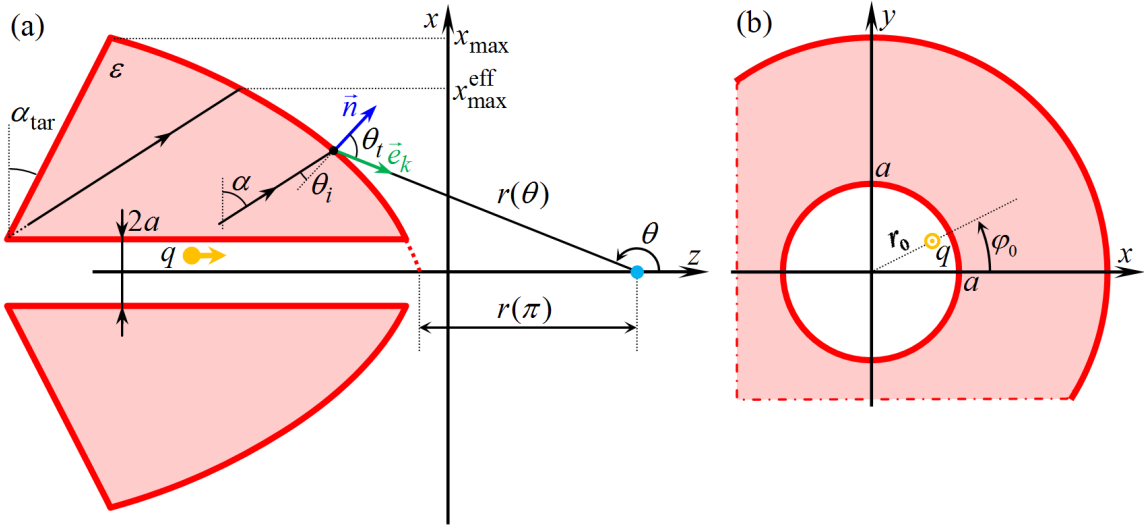


Figure 1. Geometry of the problem. (a) (zx) -cut of dielectric concentrator for Cherenkov radiation: an axisymmetric dielectric target with specific outer profile (determined by the function $r(\theta)$) and inner channel of radius a where a point charge q moves along straight trajectory shifted with respect to z -axis. Depicted parameters are discussed in the text. (b) (xy) -cut of the target (channel radius is enlarged for convenience) and position of the charge's shifted trajectory.

II. PROBLEM FORMULATION

Figure 1 shows geometry of the problem under investigation. Note that along with Cartesian frame (x, y, z) , corresponding cylindrical frame (ρ, φ, z) is introduced. A point charge q moves with constant velocity $v = \beta c$ along straight trajectory inside the channel in axisymmetric dielectric target with permittivity ε and permeability $\mu = 1$. Position of charge's trajectory is determined by r_0 and φ_0 , see Fig. 1 (b).

Cylindrical coordinates $\rho = \rho_0$, $z = z_0$ of the outer profile of the target are determined for $r_0 = 0$ as follows. A point charge moving along the axis of the structure (symmetric case) with velocity $v = \beta c$ generates Cherenkov radiation inside the target, with the corresponding rays being directed at angle $\alpha = \arcsin[1/(\sqrt{\varepsilon}\beta)]$ with respect to vertical direction, these rays are shown in Fig. 1 (a). It is supposed here that Cherenkov condition is fulfilled, $\sqrt{\varepsilon}\beta > 1$. The surface ρ_0 , z_0 is determined by the rule that all the refracted rays converge exactly to the point $x = y = 0$, $z = z_f$. Details can be found in [33, 38, 39, 41], in the issue we obtain the following φ -independent surface:

$$\begin{aligned} \rho_0(\theta) &= r(\theta) \sin(\theta), \\ z_0(\theta) &= z_f + r(\theta) \cos(\theta), \end{aligned} \quad (1)$$

where

$$r(\theta) = f(1 - \sqrt{\varepsilon}) [1 + \sqrt{\varepsilon} \sin(\alpha + \theta)]^{-1}. \quad (2)$$

Here parameter f can be called the “focal” parameter since the distance between the focal point and the “nose”

of the target $r(\pi)$ is proportional to f , i.e.

$$r(\pi) = \frac{f\beta(\sqrt{\varepsilon} - 1)}{1 - \beta}. \quad (3)$$

Therefore, the larger f the larger distance between the focus and the target. Maximum transverse size of the target x_{\max} determines minimum angle θ_{\min} , maximum angle θ_{\max} is determined by the channel radius a .

For symmetric case ($r_0 = 0$) radiation properties have been investigated in details, including dependence of field components behavior on deviation of actual charge velocity from the “designed” velocity (sensitivity) [38–40]. Moreover, a direct comparison between COMSOL simulations and the developed theory has been performed [38] and very well agreement has been observed. Below we will investigate the influence of the offset r_0 on radiation characteristics of the concentrator.

III. STRATTON-CHU FORMALISM

According to our combined approach, we utilize the Stratton-Chu formulas [42, 43] to calculate Cherenkov radiation exiting the target. Recall that these integral formulas give exact result if tangential electric and magnetic fields are determined exactly at the surface of integration (aperture S_a). In this paper, we use the form of these formulas from [43] (see also our papers [36, 37, 41])

with the outer surface of the target (1) as the aperture:

$$4\pi\vec{E}_\omega = \int_{S_a} \left\{ ik_0 [\vec{n}, \vec{H}_\omega^a] \psi + \frac{i}{k_0} \left([\vec{n}, \vec{H}_\omega^a], \vec{\nabla} \right) \vec{\nabla} \psi + \left[[\vec{E}_\omega^a, \vec{n}], \vec{\nabla} \psi \right] \right\} d\Sigma, \quad (4)$$

where ψ is a Green function,

$$\psi = \exp \left(ik_0 \tilde{R} \right) / \tilde{R}, \quad (5)$$

$$\tilde{R} = \sqrt{(x - x_0)^2 + (y - y_0)^2 + (z - z_0)^2},$$

$d\Sigma$ is a surface element of S_a . As follows from Eq. (4), EM field outside the target is determined by tangential electric and magnetic fields at S_a . We utilize the following parametrization of Cartesian coordinates of the aperture via angles θ and φ :

$$x_0(\theta, \varphi) = \rho_0(\theta) \cos \varphi, \quad y_0(\theta, \varphi) = \rho_0(\theta) \sin \varphi, \quad (6)$$

while $z_0(\theta, \varphi)$ is given by (1) together with $\rho_0(\theta)$. To calculate parameters of the surface it is convenient to use the tensor formalism by V.A. Fock [40, 44] and determine metric tensor of the surface g [40]. Then for element of the surface square we obtain $d\Sigma = \sqrt{g} d\theta d\varphi$, where

$$\sqrt{g} = \frac{-f^2(1 - \sqrt{\varepsilon})^2 \sin \theta \sqrt{1 + \sqrt{\varepsilon} \sin(\theta + \alpha)} + \varepsilon}{[1 + \sqrt{\varepsilon} \sin(\theta + \alpha)]^3}. \quad (7)$$

Components of unit normal \vec{n} are:

$$n_\rho = \frac{\sin \theta + \sqrt{\varepsilon} \cos \alpha}{\sqrt{1 + \sqrt{\varepsilon} \sin(\theta + \alpha)} + \varepsilon}, \quad (8)$$

$$n_z = \frac{\cos \theta + \sqrt{\varepsilon} \sin \alpha}{\sqrt{1 + \sqrt{\varepsilon} \sin(\theta + \alpha)} + \varepsilon}.$$

To find the fields \vec{E}_ω^a and \vec{H}_ω^a , we use the following approximate method (which was approved earlier, see, for example, [36, 38]). First, corresponding “etalon” problem should be solved to find the field in the bulk of target. For the geometry under consideration, “etalon” problem consists in determination of electromagnetic (EM) field in semi-infinite medium ($r_0 \leq \rho < \infty$) with permittivity ε having circular channel inside which a point charge q moving along shifted straight trajectory. Geometry of this problem is shown in Fig. 1 (b). Exact solution of this problem is presented in Appendix A. Note that general solution of this problem is known [23, 45]. However, it is more convenient to obtain this solution in the form used in [46, 47], which is done in the Appendix A.

From this solution in the bulk of the dielectric, Eqs. (A28) and (A29), (we put $\mu = 1$ and $\varphi_0 = 0$), one can conclude that for $\rho|s| \gg 1$ the phase term of all “modes” (summands with different ν) can be written as

$$\exp \left[ik_0 \beta^{-1} \left(z + \sqrt{\varepsilon \beta^2 - 1} \rho \right) \right], \quad (9)$$

i.e. it is the same as for symmetric case $r_0 = 0$, see Eq. (5) in [41]. From this phase one can determine corresponding rays having the following angle of refraction θ_t :

$$\sin \theta_t = \frac{-1}{\beta \sqrt{r^2 + r'^2}} \left[r \sin \theta - r' \cos \theta - \sqrt{\varepsilon \beta^2 - 1} (r \cos \theta + r' \sin \theta) \right], \quad (10)$$

where $r' = dr/d\theta$. Note that corresponding Eq. (7) in [41] contains sadly misprints.

Field (A28) and (A29) can be separated into two polarizations with respect to the plane of incidence determined by incident ray and \vec{n} , see Fig. 1. “Parallel” polarization (\parallel) contains components $E_{z\omega}$, $E_{\rho\omega}$ and $H_{\varphi\omega}$. Corresponding Fresnel coefficient is

$$T_\parallel = \frac{2 \cos \theta_i}{\cos \theta_i + \sqrt{\varepsilon} \cos \theta_t}. \quad (11)$$

“Orthogonal” polarization (\perp) contains components $H_{z\omega}$, $H_{\rho\omega}$ and $E_{\varphi\omega}$. Corresponding Fresnel coefficient is

$$T_\perp = \frac{2\sqrt{\varepsilon} \cos \theta_i}{\sqrt{\varepsilon} \cos \theta_i + \cos \theta_t}. \quad (12)$$

Angle of incidence θ_i can be obtained from Snell’s law $\sqrt{\varepsilon} \sin \theta_i = \sin \theta_t$ and (10). Unit vector of transmitted wave \vec{e}_k can be calculated as follows:

$$e_{k\rho} = n_\rho \cos \theta_t - n_z \sin \theta_t, \quad (13)$$

$$e_{kz} = n_\rho \sin \theta_t + n_z \cos \theta_t.$$

For each of two polarizations, transmitted field at the outer surface of the aperture is determined via component of the field being orthogonal to the plane of incidence, i.e. $H_{\varphi\omega}$ for \parallel -polarization and $E_{\varphi\omega}$ for \perp -polarization. For $\rho_0|s| \gg 1$ (this means that the aperture is supposed to be far enough from the charge’s trajectory) we have for the inner side of the aperture:

$$H_{\varphi\omega}^a = \frac{q\omega \exp(ik_0 z_0/\beta + i\rho_0 s - 3\pi i/4)}{i\pi v^2 \gamma^2} \sqrt{\frac{2}{\pi \rho_0 s}} \times$$

$$\times \frac{ik_0}{s^2} \left\{ -\varepsilon s I_0(r_0 \sigma_0) \tilde{A}_0^{(E2)} + 2 \sum_{\nu=1}^{\infty} I_\nu(r_0 \sigma_0) e^{\frac{i\pi(1-\nu)}{2}} \times \right. \quad (14)$$

$$\left. \times \cos(\nu\varphi) \left[\varepsilon \tilde{A}_\nu^{(E2)} \left(is - \frac{1}{2\rho_0} \right) - \frac{i\nu}{\beta \rho_0} \tilde{A}_\nu^{(H2)} \right] \right\},$$

$$E_{\varphi\omega}^a = \frac{q\omega \exp(ik_0 z_0/\beta + i\rho_0 s - 3\pi i/4)}{i\pi v^2 \gamma^2} \sqrt{\frac{2}{\pi \rho_0 s}} \times$$

$$\times \frac{ik_0}{s^2} 2 \sum_{\nu=1}^{\infty} I_\nu(r_0 \sigma_0) e^{\frac{i\pi(1-\nu)}{2}} \times \quad (15)$$

$$\times \sin(\nu\varphi) \left[i \tilde{A}_\nu^{(H2)} \left(is - \frac{1}{2\rho_0} \right) - \frac{\nu}{\beta \rho_0} \tilde{A}_\nu^{(E2)} \right],$$

where notations are given in the Appendix A. Transmitted fields at the outer surface of the aperture are:

$$\begin{aligned} H_{\varphi\omega}^a &= T_{\parallel} H_{\varphi\omega}^{a-}, & \vec{E}_{\omega}^{\parallel} &= H_{\varphi\omega}^a [\vec{e}_{\varphi}, \vec{e}_k], \\ E_{\varphi\omega}^a &= T_{\perp} E_{\varphi\omega}^{a-}, & \vec{H}_{\omega}^{\perp} &= E_{\varphi\omega}^a [\vec{e}_k, \vec{e}_{\varphi}], \end{aligned} \quad (16)$$

therefore

$$\begin{aligned} E_{\rho\omega}^a &= H_{\varphi\omega}^a e_{kz}, & E_{z\omega}^a &= -H_{\varphi\omega}^a e_{k\rho}, \\ H_{\rho\omega}^a &= -E_{\varphi\omega}^a e_{kz}, & H_{z\omega}^a &= E_{\varphi\omega}^a e_{k\rho}. \end{aligned} \quad (17)$$

From Eqs. (16) and (17), the field distribution over the outer surface of the aperture is defined and all the things needed for evaluation of integral (4) are ready.

Before presenting numerical results, let us discuss the obtained analytical results. The “mode” with number $\nu = 0$ is manifested in \parallel -polarization only. The corresponding φ -independent term in Eq. (14) gives the same field inside the target and the same field distribution over the outer target surface as non-shifted charge up to a factor $I_0(r_0\sigma_0) < 1$. Therefore, due to this zeroth “mode” the same effect of concentration will take place in non-symmetrical case (with corresponding scaling of the field). In particular, for this term transverse electric field produced by concentrator is exact zero for $\rho = 0$ [39, 40]. However, “modes” with numbers $\nu \geq 1$ will add φ -dependent field distribution over the aperture therefore altering this result. This question will be clarified in Sec. IV.

IV. NUMERICAL RESULTS AND DISCUSSION

Here we present results of EM field calculation in the area outside the target (mainly near the focal point which is of most interest) using Eq. (4). Limits of integration

over φ are from 0 to 2π , while limits of integration over θ , θ_{\min} and θ_{\max} , are determined by dimensions of the concentrator.

For evaluation of integrals (4), a numerical code was realized in MATLAB with the use of Parallel Computing Toolbox. With multicore processor, approximate time consumed for calculation of each subplot (100×100 points) in Fig. 3 was in the range 50 – 250 seconds per core depending on the model of processor.

Set of parameters used for numerical calculations is presented in Table I. First, we have put $z_f = 0$, i.e. position of the designed focus is $z = 0$. Then, for the chosen frequency ω we have determined all dimensions in units of c/ω . Channel radius was chosen to be $a = c/\omega$ and this radius determines θ_{\max} . Dielectric permittivity ε was chosen so that α is relatively large. In this case, rays inside the target propagate with relatively small angle with respect to z -axis and target longitudinal and transverse dimensions are comparable (contrary to the case of relatively small α where the target is strongly prolonged [39]).

Transverse dimensions of the target are determined by x_{\max} , see Fig 1 (a). Back slope of the target is cut by straight line determined by α_{tar} which should be smaller than α . In this case, the ray originating from the most distant (from the focus) point of the target will reach the aperture. This ray is shown in Fig. 1 (a). This ray also determines the “effective” transverse size of the target x_{\max}^{eff} which is smaller than x_{\max} . This point is taken into account in calculations: upper limit θ_{\max} is determined by x_{\max}^{eff} .

Figure 2 illustrates dependence of absolute values of $E_{x\omega}$, $E_{z\omega}$ and E_{ω} on z for $x = r_0$ and $y = 0$ (along straight line parallel to z -axis) and for three values of $r_0 = a/10, a/4, a/2$. Black (thickest) line shows field generated by 0th (symmetrical with respect to φ) “mode” in Eq. (14). Recall that this “mode” gives the same field as in symmetrical case (only scaled by the factor $I_0(r_0\sigma_0)$). One can see that transverse field $E_{x\omega}$ is negligible near z -axis, which is natural due to the symmetry considerations, while longitudinal field $E_{z\omega}$ is dominant. These are results obtained earlier [39, 40].

Cyan (thinner) line in Fig. 2 shows field generated by two “modes” (0th and 1st) of “effective surface currents”, while dashed magenta line shows field generated by three those “modes”, 0th, 1st and 2nd. As one can see, even for $r_0 = a/2$ contribution of the 2nd “mode” is negligible, therefore we can restrict ourselves by taking into account mentioned three modes in Eqs. (14) and (15).

To illustrate main results we will plot two-dimensional field distributions. Figure 3 shows two-dimensional distribution of longitudinal ($E_{z\omega}$) and transverse ($E_{\rho\omega}$) components over xy -plane for symmetric case $r_0 = 0$. Note that this is not a principally new result but a new illustration of previous results obtained in [38–40]. As one can clearly see from Fig. 3, transverse field is exact zero on the symmetry axis while longitudinal field is maximal here. Transverse field quickly increases while observation

Table I. Parameters of numerical calculations.

Parameter	Value
ω	$2\pi \cdot 100\text{GHz}$
λ	0.3cm
$c/\omega = \lambda/(2\pi)$	0.05cm
β	0.8
“Focal” parameter f	$500c/\omega \approx 24\text{cm}$
$r(\pi)$	$540c/\omega \approx 26\text{cm}$
q	1nC
x_{\max}	$500c/\omega \approx 24\text{cm}$
x_{\max}^{eff}	$340c/\omega \approx 16\text{cm}$
a	c/ω
θ_{\min}	162°
θ_{\max}	179°
ε	1.6
α	80°
α_{tar}	73°

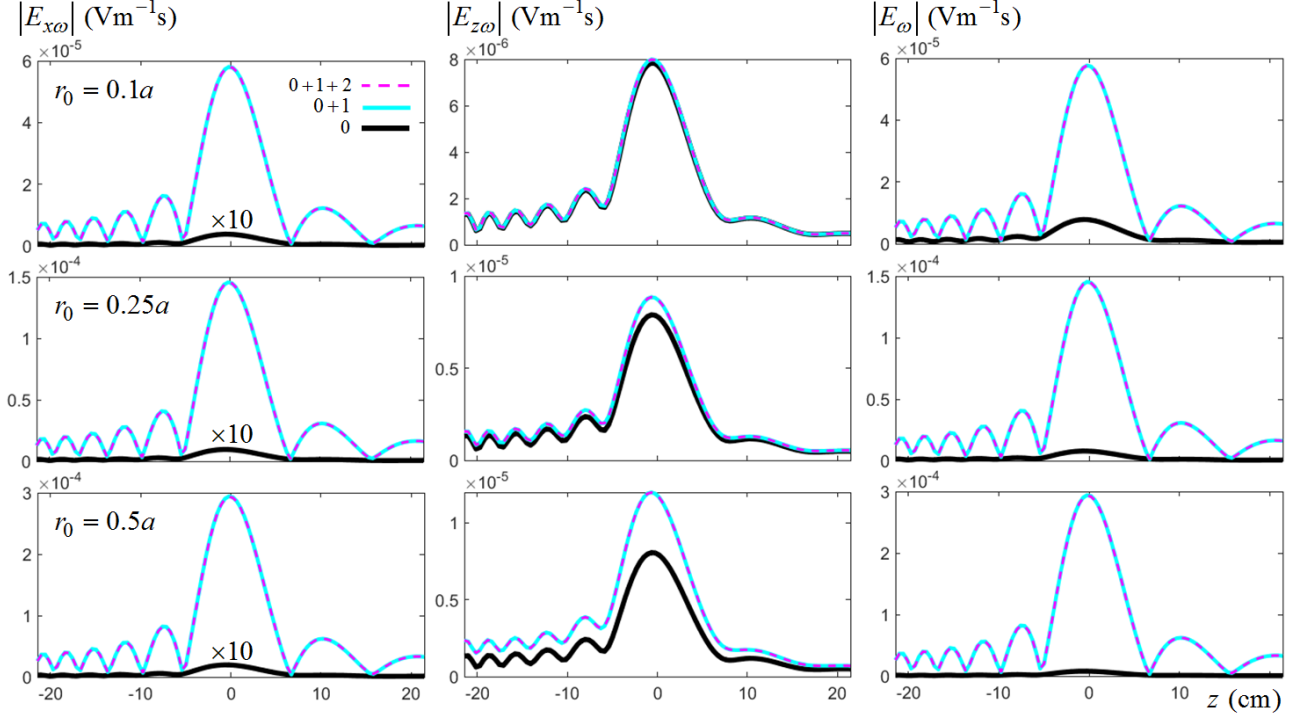


Figure 2. Field behavior along the line parallel to z -axis and having offset r_0 in x -direction. Black (thickest) line (multiplied by factor 10 in the left column to be recognized from zero) corresponds to the contribution of the term with $\nu = 0$ in Eq. (14). Cyan (thinner) and magenta (dashed) lines correspond to the contribution of two terms (with $\nu = 0, 1$) and three terms (with $\nu = 0, 1, 2$), correspondingly, in Eqs. (14) and (15). Top row is for $r_0 = a/10$, middle row is for $r_0 = a/4$ and bottom row is for $r_0 = a/2$.

point is shifted from z -axis and has its maximum value around two times larger compared to maximum of $E_{z\omega}$. In all cases, fields strongly decrease with an increase in shift of the observation plane from the focal plane $z = 0$. Total field is practically determined by transverse field excluding mentioned central area (a circle with radius $\approx 3a$) where longitudinal field is dominant.

Field distribution for the case with a charge shifted from z -axis is shown in Fig. 4 for the focal plane $z = z_f = 0$. Note that tendencies in field behavior connected with shift of observation plane from the focal plane ($z < 0$ or $z > 0$) are practically the same as for symmetrical case: decrease in field magnitude and smoothing. Also magnitudes of transverse and longitudinal fields differ approximately by factor 5 and increase almost linearly with increasing r_0 .

The most interesting feature is occurred in longitudinal field (see Fig. 4, left column). For relatively small offset ($r_0 = a/10$), this field is strongly asymmetric with respect to $x = 0$. The stronger peak is located in the area $x > 0$, i.e. in the area where shifted charge propagates (recall that $\varphi_0 = 0$, therefore a charge is shifted to positive x). With an increase in r_0 these peaks become more symmetrical ($r_0 = a/4$), and for relatively large offset ($r_0 = a/2$) we have two almost symmetrical peaks located approximately at $x = 6.7a$ and $x = -8.7a$, i.e. far enough from the charge trajectory. More detailed

position of the discussed peaks is shown in Fig. 5.

In turn, transverse field (see Fig. 4, right column) also has an essential asymmetry for relatively small offsets ($r_0 = a/10$). It is worth noting that the peak of transverse field is shifted in opposite direction compared to the shift of the charge trajectory, its approximate location is $x = -2.3a$ (see Fig. 5 for details). Therefore in this case (small offset) one can potentially detect these peaks separately: the peak of $E_{z\omega}$ for $x > 0$ and the peak of $E_{\rho\omega}$ for $x < 0$. For larger offsets, the peak of $E_{\rho\omega}$ becomes practically symmetric in both x and y direction, is located nearly in the center and dominates the longitudinal peak.

Possible applications of the presented dielectric concentrator would lie in the area of beam diagnostics and beam manipulation. Since strong field concentration takes place in the focal plane near the focal point, sensitivity and accuracy of mentioned diagnostics can be essentially increased. For example, peculiarities of field distribution for $r_0 \neq 0$ can be used for determination of beam shift and positioning the beam to the axis of the structure. Note that difference between magnitudes of two peaks of top plot in Fig. 5 depends on r_0 . For $r_0 = a/10$ left peak magnitude is about 50% of the right peak magnitude while for $r_0 = a/2$ left peak magnitude is about 90% of the right peak magnitude. Moreover, these peaks are shifted for several values of a (in our case from

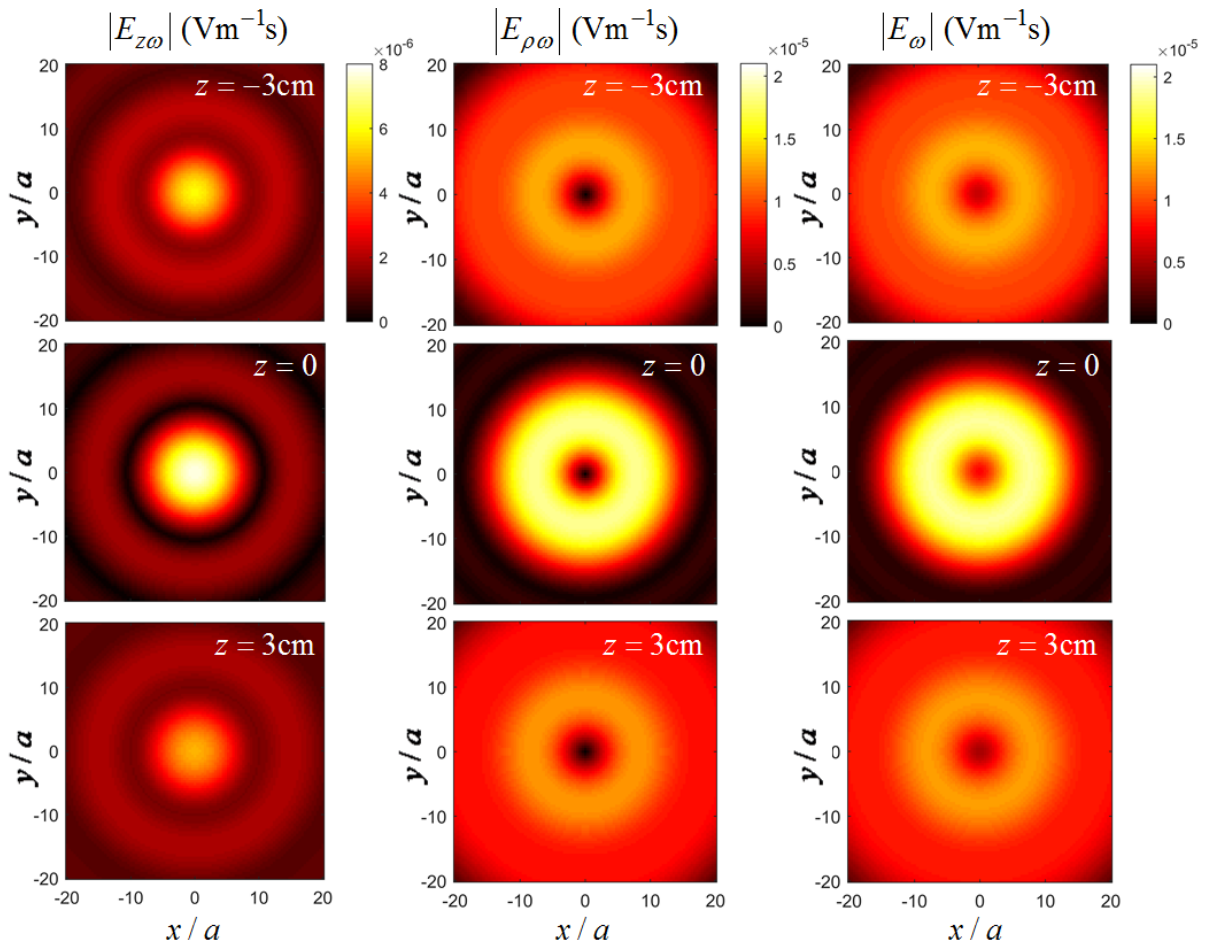


Figure 3. Two dimensional distribution of absolute values of longitudinal ($E_{z\omega}$), transverse ($E_{\rho\omega}$) and total (E_{ω}) field over xy -plane for symmetrical case $r_0 = 0$. Plane $z = z_f = 0$ is the focal plane of the concentrator. Calculation parameters are given in Table I.

≈ 5 to ≈ 8) from the axis thus simplifying the detection of the field.

If the bunch is well aligned along the axis ($r_0 = 0$), it experiences influence of longitudinal field ($E_{z\omega}$) only, see Fig. 3. Interaction between the bunch and strongly concentrated radiated field can lead to longitudinal modulation of the bunch. If the bunch is shifted ($r_0 \neq 0$), it is affected by strong transverse field in the focal plane. Therefore, the concentrator can operate as a transverse kicker in this case.

V. CONCLUSION

In the present paper, we have presented analytical and numerical investigation of EM radiation produced by a point charge moving through the dielectric concentrator for Cherenkov radiation (see [33]) for the case of off-axis charge propagation. The problem has been solved using original combined approach (developed and verified in our previous papers) suitable for investigation of radiation from various dielectric targets of finite size with

several sharp interfaces. It is worth noting that this approach possesses asymptotic accuracy with respect to ratio between wavelength and transverse size of target.

Contrary to symmetric case (a charge moves exactly along the structure axis) considered in our papers earlier, here strong asymmetry of the field distribution near the focal plane is observed and illustrated. For example, with an increase in charge offset, peak of longitudinal field is first shifted in the direction of charge shift and then is divided into two peaks. Since difference between magnitudes of these peaks depend on charge offset, detection of these peaks can be possibly used for determination of charge offset and charge alignment inside the structure. Note that transverse position of the discussed peaks is several channel radii, therefore they can be potentially detected without a need to deflect or damp the charge. Due to the charge offset, strong transverse electric field (which is several times larger compared to the longitudinal field) is generated near the concentrator symmetry axis. As was shown, the peak of this field is also shifted with change in charge offset however in opposite direction. For small offset, due to opposite shift of the lon-

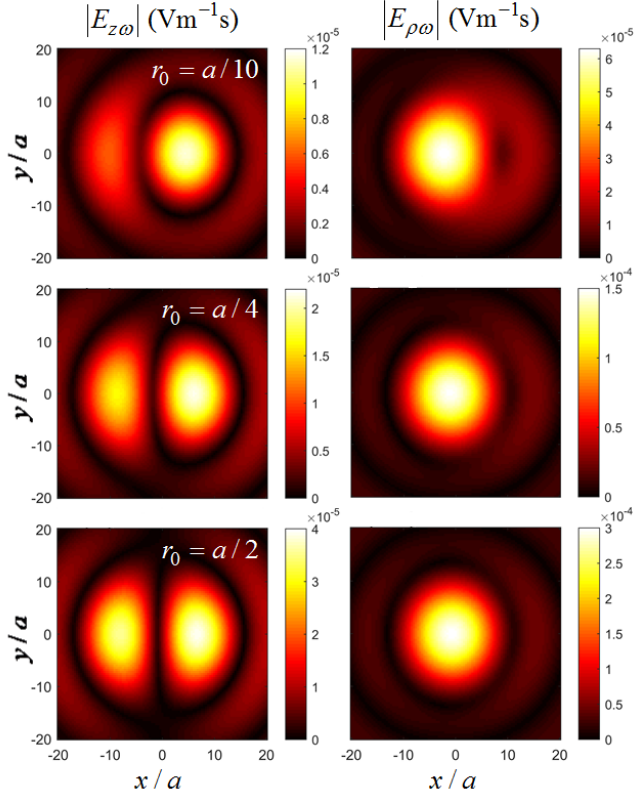


Figure 4. Two dimensional distribution of absolute values of longitudinal ($E_{z\omega}$) and transverse ($E_{\rho\omega}$) field over xy -plane in the focal plane of the concentrator ($z = 0$) for three values of charge's shift $r_0 = a/10, a/4, a/2$. Calculation parameters are given in Table I.

gitudinal field peak and the transverse field peak, these field components can be possibly detected independently. Moreover, strong transverse field can be used as an all-dielectric transverse kicker.

VI. ACKNOWLEDGMENTS

This work was supported by Russian Foundation for Basic Research (RFBR), grant No. 17-52-04107.

Appendix A: Solution of “etalon” problem

For the case under consideration, geometry of “etalon” problem is shown in Fig. 1 (b). Within this section, cylindrical frame (ρ, φ, z) is utilized. One should find the field in semi-infinite medium ($r_0 \leq \rho < \infty$) with permittivity ϵ and permeability μ having a cylindrical channel where a charge propagates along shifted trajectory. It is supposed that the trajectory is shifted in $\varphi = \varphi_0$ direction and r_0 is the value of this shift. In addition, we will refer to the area $\rho \leq a$ as “area 1” and to the area $\rho \geq a$ as “area 2”. As was mentioned above, despite of the fact

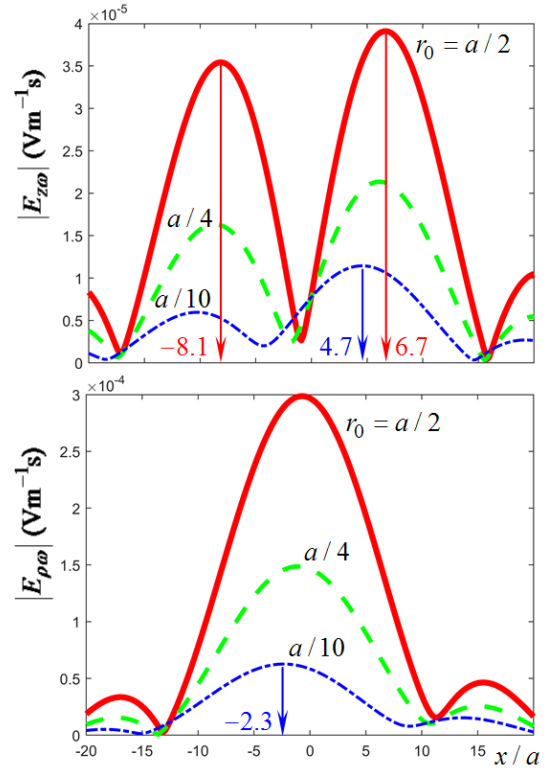


Figure 5. Dependence of absolute values of longitudinal ($E_{z\omega}$) and transverse ($E_{\rho\omega}$) field over x for $y = z = 0$ for three values of charge's shift $r_0 = a/10, a/4, a/2$. Calculation parameters are the same as in Fig. 4.

that general solution of this problem is known [23, 45] it is useful to obtain it in more convenient form, similar to those in [46, 47].

The problem is solved for Fourier transforms of field components, for example:

$$\vec{E}_\omega = \frac{1}{2\pi} \int_{-\infty}^{+\infty} \vec{E} \exp(i\omega t) dt. \quad (\text{A1})$$

Charge and current densities have the form

$$\rho_q = q \frac{\delta(\rho - r_0)}{\rho} \delta(\varphi - \varphi_0) \delta(z - vt), \quad j = \rho_q v, \quad \vec{j} = j \vec{e}_z. \quad (\text{A2})$$

Here $v = \beta c$ and $\delta(\varphi - \varphi_0)$ means 2π -periodic function with corresponding δ singularity in each period. This function can be decomposed in Fourier series as follows:

$$\delta(\varphi - \varphi_0) = \frac{1}{2\pi} \sum_{\nu=-\infty}^{+\infty} \exp(-i\nu(\varphi - \varphi_0)). \quad (\text{A3})$$

For radial part in (A2) the following decomposition holds for arbitrary integer ν [48]:

$$\frac{\delta(\rho - r_0)}{\rho} = \int_0^{+\infty} J_\nu(\rho\xi) J_\nu(r_0\xi) \xi d\xi, \quad (\text{A4})$$

where J_ν is Bessel function of order ν . Fourier transforms (A1) of the sources (A2) have the form:

$$\rho_{q\omega} = \frac{q}{2\pi v} \frac{\delta(\rho - r_0)}{\rho} \delta(\varphi - \varphi_0) \exp\left(i\frac{\omega z}{v}\right), \quad j_\omega = v\rho_{q\omega}. \quad (\text{A5})$$

From Maxwell's equations for magnitudes of Fourier harmonics

$$\begin{aligned} \text{rot} \vec{E}_\omega &= ik_0 \mu \vec{H}_\omega, \\ \text{rot} \vec{H}_\omega &= -ik_0 \varepsilon \vec{E}_\omega + \frac{4\pi}{c} \vec{j}_\omega, \\ \varepsilon \text{div} \vec{E}_\omega &= 4\pi \rho_{q\omega}, \quad \text{div} \vec{H}_\omega = 0, \end{aligned} \quad (\text{A6})$$

$k_0 = \omega/c$, one can obtain the following two equations for longitudinal components of electric and magnetic field [46, 47]:

$$\begin{aligned} \Delta E_{z\omega} + k_0^2 \varepsilon \mu E_{z\omega} &= \frac{4\pi}{\varepsilon} \frac{\partial \rho_{q\omega}}{\partial z} - \frac{4\pi i \omega \mu}{c^2} j_\omega, \\ \Delta H_{z\omega} + k_0^2 \varepsilon \mu H_{z\omega} &= 0, \end{aligned} \quad (\text{A7})$$

where

$$\Delta = \frac{\partial^2}{\partial \rho^2} + \frac{1}{\rho} \frac{\partial}{\partial \rho} + \frac{1}{\rho^2} \frac{\partial}{\partial \varphi^2} + \frac{\partial^2}{\partial z^2}, \quad (\text{A8})$$

and the following expressions for the rest of the field components:

$$\begin{aligned} E_{\rho\omega} &= \frac{i}{k_0 \varepsilon} \left(\frac{1}{\rho} \frac{\partial H_{z\omega}}{\partial \varphi} - \frac{\partial H_{\varphi\omega}}{\partial z} \right), \\ H_{\rho\omega} &= \frac{-i}{k_0 \mu} \left(\frac{1}{\rho} \frac{\partial E_{z\omega}}{\partial \varphi} - \frac{\partial E_{\varphi\omega}}{\partial z} \right), \end{aligned} \quad (\text{A9})$$

$$\begin{aligned} \left(\frac{\partial^2}{\partial z^2} + k_0^2 \varepsilon \mu \right) H_{\varphi\omega} &= \frac{1}{\rho} \frac{\partial^2 H_{z\omega}}{\partial z \partial \varphi} + ik_0 \varepsilon \frac{\partial E_{z\omega}}{\partial \rho}, \\ \left(\frac{\partial^2}{\partial z^2} + k_0^2 \varepsilon \mu \right) E_{\varphi\omega} &= \frac{1}{\rho} \frac{\partial^2 E_{z\omega}}{\partial z \partial \varphi} - ik_0 \mu \frac{\partial H_{z\omega}}{\partial \rho}. \end{aligned} \quad (\text{A10})$$

Since z -dependence in sources (A5) is $\exp(i\omega z/v)$, field components should have the same dependence, i.e.:

$$\left\{ \vec{E}_\omega, \vec{H}_\omega \right\} = \left\{ \vec{\tilde{E}}_\omega, \vec{\tilde{H}}_\omega \right\} \exp\left(i\frac{\omega z}{v}\right), \quad (\text{A11})$$

therefore $\partial/\partial z \rightarrow ik_0/\beta$ in Eqs. (A7), (A8), (A9) and (A10). Moreover, since $\vec{\tilde{E}}_\omega$ should be 2π periodic function, it should be decomposed in Fourier series, similar to (A3):

$$\vec{\tilde{E}}_\omega = \sum_{\nu=-\infty}^{+\infty} \vec{\tilde{E}}_{\omega\nu} \exp(-i\nu\varphi), \quad (\text{A12})$$

therefore $\partial/\partial \varphi \rightarrow -i\nu$ in Eqs. (A7), (A8), (A9) and (A10). Taking into account all these considerations, we obtain from Eq. (A7)

$$\begin{aligned} \left[\frac{\partial^2}{\partial \rho^2} + \frac{1}{\rho} \frac{\partial}{\partial \rho} + s^2 - \frac{\nu^2}{\rho^2} \right] \tilde{E}_{z\omega\nu} &= 4\pi \tilde{Q}_{\omega\nu}, \\ \left[\frac{\partial^2}{\partial \rho^2} + \frac{1}{\rho} \frac{\partial}{\partial \rho} + s^2 - \frac{\nu^2}{\rho^2} \right] \tilde{H}_{z\omega\nu} &= 0, \end{aligned} \quad (\text{A13})$$

$$\tilde{Q}_{\omega\nu} = \frac{iq\sigma^2}{4\pi^2\omega\epsilon} e^{i\nu\varphi_0} \int_0^{+\infty} J_\nu(\rho\xi) J_\nu(r_0\xi) \xi d\xi, \quad (\text{A14})$$

$$s^2 = \frac{k_0^2}{\beta^2} (\varepsilon\mu\beta^2 - 1), \quad \sigma^2 = -s^2. \quad (\text{A15})$$

Particular solution (this solution will be supported by upper index (i) and will be further referred to as “incident” field) of Eq. (A13) is $\tilde{H}_{z\omega\nu}^{(i)} = 0$,

$$\tilde{E}_{z\omega\nu}^{(i)} = \frac{iq\sigma^2}{\pi\omega\epsilon} e^{i\nu\varphi_0} \int_0^{+\infty} \frac{J_\nu(\rho\xi) J_\nu(r_0\xi)}{s^2 - \xi^2} \xi d\xi. \quad (\text{A16})$$

We will further suppose that “incident” field (A16) is determined inside the vacuum channel (area 1, $\rho \leq a$), where $\varepsilon = \mu = 1$, $\sigma^2 = \sigma_0^2 = k_0^2 \beta^{-2} (1 - \beta^2) = k_0^2 \beta^{-2} \gamma^{-2}$, γ is Lorentz factor. Integral over ξ in (A16) is tabular [49], and we obtain:

$$\tilde{E}_{z\omega\nu}^{(i)} = \frac{-iq\sigma_0^2}{\pi\omega} e^{i\nu\varphi_0} \begin{cases} K_\nu(r_0\sigma_0) I_\nu(\rho\sigma_0) & \text{for } \rho \leq r_0, \\ I_\nu(r_0\sigma_0) K_\nu(\rho\sigma_0) & \text{for } \rho \geq r_0, \end{cases} \quad (\text{A17})$$

where I_ν and K_ν are modified Bessel and Hankel functions, correspondingly, $\sigma_0 = \sqrt{\sigma^2}$, $\text{Re}\sqrt{\cdot} > 0$.

“Scattered” field is the general solution of homogeneous equations in (A13) which can be easily transformed to Bessel or modified Bessel equations. Inside the vacuum channel (area 1, $\rho \leq a$, $\sigma = \sigma_0$), it is convenient to decompose this general solution over linearly independent solutions of modified Bessel equation, $I_\nu(\rho\sigma_0)$ and $K_\nu(\rho\sigma_0)$. Since it should contain no singularity for $\rho \rightarrow 0$, we obtain:

$$\tilde{E}_{z\omega\nu}^{(1)} A_\nu^{(E1)} I_\nu(\rho\sigma_0), \quad \tilde{H}_{z\omega\nu}^{(1)} A_\nu^{(H1)} I_\nu(\rho\sigma_0). \quad (\text{A18})$$

Outside the vacuum channel (area 2, $\rho \geq a$), it is convenient to decompose this general solution over linearly independent solutions of Bessel equation, $H_\nu^{(1)}(\rho s)$ and $H_\nu^{(2)}(\rho s)$, where $s = \sqrt{s^2}$, $\text{Im}\sqrt{\cdot} > 0$. Since it should represent an outgoing wave, we obtain:

$$\tilde{E}_{z\omega\nu}^{(2)} A_\nu^{(E2)} H_\nu^{(1)}(\rho s), \quad \tilde{H}_{z\omega\nu}^{(2)} A_\nu^{(H2)} H_\nu^{(1)}(\rho s). \quad (\text{A19})$$

Boundary conditions (continuity of $\tilde{E}_{z\omega\nu}$, $\tilde{H}_{z\omega\nu}$, $\tilde{E}_{\varphi\omega\nu}$ and $\tilde{H}_{\varphi\omega\nu}$) for $\rho = a$ result in 2×2 linear system for unknown $A_\nu^{(E1,2)}$ and $A_\nu^{(H1,2)}$. The determinant is:

$$\begin{aligned} \Delta_\nu &= [\nu(\beta a)^{-1} I_\nu(\sigma_0^2 + s^2)]^2 - \\ &- \frac{[\sigma_0^2 s \varepsilon H'_\nu I_\nu + s^2 \sigma_0 I'_\nu H_\nu][\sigma_0^2 s \mu H'_\nu I_\nu + s^2 \sigma_0 I'_\nu H_\nu]}{H_\nu^2}, \end{aligned} \quad (\text{A20})$$

where

$$\begin{aligned} I_\nu &\equiv I_\nu(a\sigma_0), \quad H_\nu \equiv H_\nu^{(1)}(as), \\ I'_\nu &\equiv \left. \frac{dI_\nu(\xi)}{d\xi} \right|_{\xi=a\sigma_0}, \quad H'_\nu \equiv \left. \frac{dH_\nu^{(1)}(\xi)}{d\xi} \right|_{\xi=as}. \end{aligned} \quad (\text{A21})$$

Coefficients are expressed as follows:

$$\tilde{A}_\nu^{(E1)} = \frac{1}{\Delta_\nu H_\nu^2} \left\{ [\nu(\beta a)^{-1} I_\nu(\sigma_0^2 + s^2)]^2 H_\nu^2 K_\nu I_\nu^{-1} + [\sigma_0^2 s \mu H'_\nu I_\nu + s^2 \sigma_0 I'_\nu H_\nu] [\sigma_0^2 s \varepsilon H'_\nu K_\nu + s^2 \sigma_0 K'_\nu H_\nu] \right\}, \quad (\text{A22})$$

$$\tilde{A}_\nu^{(H1)} = \frac{\nu I_\nu(\sigma_0^2 + s^2)}{i\beta a \Delta_\nu H_\nu} \left\{ [\sigma_0^2 s \varepsilon H'_\nu K_\nu + s^2 \sigma_0 K'_\nu H_\nu] + K_\nu I_\nu^{-1} [\sigma_0^2 s \varepsilon H'_\nu I_\nu + s^2 \sigma_0 I'_\nu H_\nu] \right\}, \quad (\text{A23})$$

where, in addition to (A21),

$$K_\nu \equiv K_\nu(a\sigma_0), \quad K'_\nu \equiv \left. \frac{dK_\nu(\xi)}{d\xi} \right|_{\xi=a\sigma_0}, \quad (\text{A24})$$

$$\tilde{A}_\nu^{(E2)} = \tilde{A}_\nu^{(E1)} \frac{I_\nu}{H_\nu} + \frac{K_\nu}{H_\nu}, \quad \tilde{A}_\nu^{(H2)} = \tilde{A}_\nu^{(H1)} \frac{I_\nu}{H_\nu} \quad (\text{A25})$$

and

$$A_\nu = \tilde{A}_\nu \frac{q\omega}{i\pi v^2 \gamma^2} \exp(i\nu\varphi_0) I_\nu(r_0\sigma_0). \quad (\text{A26})$$

Using the properties of Bessel functions, $I_{-\nu} = I_\nu$, $K_{-\nu} = K_\nu$, $H_{-\nu} = \exp(i\nu\pi)H_\nu$, one can show that

$$\Delta_{-\nu} = \Delta_\nu, \quad \tilde{A}_{-\nu}^{(E1)} = \tilde{A}_\nu^{(E1)}, \quad \tilde{A}_{-\nu}^{(H1)} = -\tilde{A}_\nu^{(H1)}, \quad (\text{A27})$$

$$\tilde{A}_{-\nu}^{(E2)} = \frac{\tilde{A}_\nu^{(E2)}}{\exp(i\nu\pi)}, \quad \tilde{A}_{-\nu}^{(H2)} = \frac{-\tilde{A}_\nu^{(E2)}}{\exp(i\nu\pi)}.$$

Using (A27), one can present “scattered” field in the bulk of medium (area 2) in the following convenient form:

$$E_{z\omega}^{(2)} = \frac{q\omega \exp(i\omega z/v)}{i\pi v^2 \gamma^2} \left\{ I_0(r_0\sigma_0) H_0^{(1)}(\rho s) \tilde{A}_0^{(E2)} + 2 \sum_{\nu=1}^{\infty} \cos[\nu(\varphi - \varphi_0)] I_\nu(r_0\sigma_0) \tilde{A}_\nu^{(E2)} H_\nu^{(1)}(\rho s) \right\}, \quad (\text{A28})$$

$$H_{z\omega}^{(2)} = \frac{q\omega \exp(i\omega z/v)}{i\pi v^2 \gamma^2} \times 2 \sum_{\nu=1}^{\infty} \sin[\nu(\varphi - \varphi_0)] I_\nu(r_0\sigma_0) i \tilde{A}_\nu^{(H2)} H_\nu^{(1)}(\rho s). \quad (\text{A29})$$

- [1] P. A. Čerenkov, Phys. Rev. **52**, 378 (1937).
- [2] I. E. Tamm and I. M. Frank, Compt. Rend. Acad. Sci. URSS **14**, 109 (1937).
- [3] J. V. Jelley, *Čerenkov Radiation and its Applications* (Pergamon, 1958).
- [4] V. P. Zrelov, *Vavilov-Cherenkov Radiation in High-Energy Physics* (Israel Program for Scientific Translations, Jerusalem, 1970).
- [5] A. E. Spinelli, F. Boschi, D. D’Ambrosio, L. Calderan, M. Marengo, A. Fenzi, M. Menegazzi, A. Sbarbati, A. Del Vecchio, and R. Calandrino, Nucl. Instr. Meth. Phys. Res. A **648**, S310 (2011).
- [6] A. E. Spinelli, M. Ferdeghini, C. Cavedon, E. Zivelonghi, R. Calandrino, A. Fenzi, A. Sbarbati, and F. Boschi, Journal of Biomedical Optics **18**, 020502 (2013).
- [7] S. Antipov, C. Jing, A. Kanareykin, J. E. Butler, V. Yakimenko, M. Fedurin, K. Kusche, and W. Gai, Appl. Phys. Lett. **100**, 132910 (2012).
- [8] S. Antipov, C. Jing, M. Fedurin, W. Gai, A. Kanareykin, K. Kusche, P. Schoessow, V. Yakimenko, and A. Zholents, Phys. Rev. Lett. **108**, 144801 (2012).
- [9] C. Jing, S. Antipov, M. Conde, W. Gai, G. Ha, W. Liu, N. Neveu, J. Power, J. Qiu, J. Shi, D. Wang, and E. Wisniewski, Nuclear Instruments and Methods in Physics Research Section A: Accelerators, Spectrometers, Detectors and Associated Equipment **898**, 72 (2018).
- [10] B. D. O’Shea, G. Andonian, S. Barber, K. Fitzmorris, S. Hakimi, J. Harrison, P. D. Hoang, M. J. Hogan, B. Naranjo, O. B. Williams, V. Yakimenko, and J. Rosenzweig, Nature Communications **7**, 12763 (2016).
- [11] S. Antipov, M. Babzien, C. Jing, M. Fedurin, W. Gai, A. Kanareykin, K. Kusche, V. Yakimenko, and A. Zholents, Phys. Rev. Lett. **111**, 134802 (2013).
- [12] S. N. Galyamin, A. V. Tyukhtin, S. Antipov, and S. S. Baturin, Opt. Express **22**, 8902 (2014).
- [13] S. Antipov, C. Jing, S. Baryshev, A. Kanareykin, D. Wang, W. Gai, A. Zholents, and M. Fedurin, in *Proceedings of the 6th International Particle Accelerator Conference (IPAC2015)* (2015) pp. 1029–1931.
- [14] S. Antipov, S. V. Baryshev, R. Kostin, S. Baturin, J. Qiu, C. Jing, C. Swinson, M. Fedurin, and D. Wang, Applied Physics Letters **109**, 142901 (2016).
- [15] D. Wang, X. Su, L. Yan, Y. Du, Q. Tian, Y. Liang, L. Niu, W. Huang, W. Gai, C. Tang, and S. Antipov, Applied Physics Letters **111**, 174102 (2017), <https://doi.org/10.1063/1.4999959>.
- [16] A. P. Potylitsyn, S. Y. Gogolev, D. V. Karlovets, G. A. Naumenko, Y. A. Popov, M. V. Shevelev, and L. G. Sukhikh, in *Proceedings of IPAC’10* (2010) pp. 1074–1076.
- [17] M. Bergamaschi, R. Kieffer, R. Jones, T. Lefevre, S. Mazzoni, M. Billing, J. Conway, J. Shanks, P. Karataev, and L. Bobb, in *Proc. of International Particle Accelerator Conference (IPAC’17), Copenhagen, Denmark, 14-19 May, 2017*, International Particle Accelerator Conference No. 8 (JACoW, Geneva, Switzerland, 2017) pp. 400–403, <https://doi.org/10.18429/JACoW-IPAC2017-MOPAB118>.
- [18] M. Bergamaschi, R. Kieffer, R. Jones, T. Lefevre, S. Mazzoni, V. V. Bleko, A. S. Konkov, J. S. Markova, A. P. Potylitsyn, P. Karataev, K. Lekontsev, L. Bobb, L. Bartnik, M. Billing, J. Conway, M. Forster, Y. Padilla Fuentes, J. Shanks, and S. Wang, in *Proc. 9th International Particle Accelerator Conference (IPAC’18), Vancouver, BC, Canada, April 29-May 4, 2018*, International Particle Accelerator Conference No. 9 (JACoW Publishing, Geneva, Switzerland, 2018) pp. 2005–2008, <https://doi.org/10.18429/JACoW-IPAC2018-WEPAF074>.
- [19] R. Kieffer, L. Bartnik, M. Bergamaschi, V. V. Bleko,

- M. Billing, L. Bobb, J. Conway, M. Forster, P. Karataev, A. S. Konkov, R. O. Jones, T. Lefevre, J. S. Markova, S. Mazzoni, Y. Padilla Fuentes, A. P. Potylitsyn, J. Shanks, and S. Wang, *Phys. Rev. Lett.* **121**, 054802 (2018).
- [20] T. Takahashi, Y. Shibata, K. Ishi, M. Ikezawa, M. Oyama, and Y. Kondo, *Phys. Rev. E* **62**, 8606 (2000).
- [21] N. Sei, T. Sakai, K. Hayakawa, T. Tanaka, Y. Hayakawa, K. Nakao, K. Nogami, and M. Inagaki, *Physics Letters A* **379**, 2399 (2015).
- [22] N. Sei and T. Takahashi, *Scientific Reports* **7**, 17440 (2017).
- [23] B. M. Bolotovskii, *Physics-Uspekhi* **62**, 201 (1957).
- [24] B. M. Bolotovskii, *Physics-Uspekhi* **4**, 781 (1962).
- [25] G. N. Afanasiev, *Vavilov-Cherenkov and Synchrotron Radiation: Foundations and Applications* (Springer, 2004).
- [26] A. A. Tishchenko, A. P. Potylitsyn, and M. N. Strikhanov, *Phys. Rev. E* **70**, 066501 (2004).
- [27] D. V. Karlovets, *JETP* **113**, 27 (2011).
- [28] M. Shevelev, A. Konkov, and A. Aryshev, *Phys. Rev. A* **92**, 053851 (2015).
- [29] A. P. Potylitsyn, S. Y. Gogolev, and L. G. Sukhikh, *Nuclear Instruments and Methods in Physics Research Section B: Beam Interactions with Materials and Atoms* **402**, 139 (2017).
- [30] A. Tishchenko, D. Y. Sergeeva, A. Ponomarenko, and M. Strikhanov, *Nuclear Instruments and Methods in Physics Research Section B: Beam Interactions with Materials and Atoms* **402**, 177 (2017).
- [31] S. Y. Gogolev and A. P. Potylitsyn, *Physics Letters A* **383**, 888 (2019).
- [32] E. S. Belonogaya, A. V. Tyukhtin, and S. N. Galyamin, *Phys. Rev. E* **87**, 043201 (2013).
- [33] S. N. Galyamin and A. V. Tyukhtin, *Phys. Rev. Lett.* **113**, 064802 (2014).
- [34] E. S. Belonogaya, S. N. Galyamin, and A. V. Tyukhtin, *J. Opt. Soc. Am. B* **32**, 649 (2015).
- [35] A. V. Tyukhtin, E. S. Belonogaya, and S. N. Galyamin, in *Proceedings of the 6th International Particle Accelerator Conference (IPAC2016)* (2016) pp. 1626–1628.
- [36] A. V. Tyukhtin, S. N. Galyamin, and V. V. Vorobev, *Phys. Rev. A* **99**, 023810 (2019).
- [37] A. V. Tyukhtin, V. V. Vorobev, S. N. Galyamin, and E. S. Belonogaya, *Phys. Rev. Accel. Beams* **22**, 012802 (2019).
- [38] S. Galyamin, A. Tyukhtin, and V. Vorobev, *Journal of Instrumentation* **13**, C02029 (2018).
- [39] S. N. Galyamin, A. V. Tyukhtin, V. V. Vorobev, G. A. A., and E. S. Belonogaya, in *Proceedings of the 25th Russian Particle Accelerator Conference (RuPAC2016)* (2016) pp. 316–318.
- [40] S. N. Galyamin, A. V. Tyukhtin, and V. V. Vorobev, *Nuclear Instruments and Methods in Physics Research Section B: Beam Interactions with Materials and Atoms* **402**, 144 (2017).
- [41] S. N. Galyamin and A. V. Tyukhtin, *Nuclear Instruments and Methods in Physics Research Section B: Beam Interactions with Materials and Atoms* **402**, 185 (2017).
- [42] J. A. Stratton and L. J. Chu, *Phys. Rev.* **56**, 99 (1939).
- [43] A. Z. Fradin, *Microwave Antennas* (Pergamon, 1961).
- [44] V. A. Fok, *Electromagnetic diffraction and propagation problems* (Pergamon Press, 1965).
- [45] L. S. Bogdankevich and B. M. Bolotovskii, *JETP* **5**, 1157 (1957).
- [46] K.-Y. Ng, *Phys. Rev. D* **42**, 1819 (1990).
- [47] A. M. Altmark, A. D. Kanareykin, and I. L. Sheinman, *Technical Physics* **50**, 87 (2005).
- [48] G. A. Korn and T. M. Korn, *Mathematical Handbook for Scientists and Engineers* (Mineola, New York: Dover Publikations, 2013).
- [49] A. P. Prudnikov, Y. A. Brychkov, and O. I. Marichev, *Integrals and Series, Vol. 2, Special functions* (Gordon & Breach Sci. Publ., New York, 1986).